

---

# **EXPERIMENTAL DESIGN FOR COMBINATORIAL AND HIGH THROUGHPUT MATERIALS DEVELOPMENT**

---

Edited by

**JAMES N. CAWSE**

*GE Global Research*

 **WILEY-  
INTERSCIENCE**

A JOHN WILEY & SONS, INC., PUBLICATION

## CHAPTER 5

---

# COMBINATORIAL MAPPING OF POLYMER BLENDS PHASE BEHAVIOR

---

ALAMGIR KARIM, AMIT SEHGAL, AND ERIC J. AMIS  
*National Institute of Standards and Technology*

J. CARSON MEREDITH  
*Georgia Institute of Technology*

### 5.1 INTRODUCTION

Combinatorial methods (CM) and high-throughput measurements of relevant chemical and physical properties, when combined with the informatics approaches of data mining and automated analysis, allow for efficient development of structure–processing–property relationships. The benefits include efficient characterization of novel regimes of thermodynamic and kinetic behavior (knowledge discovery) and accelerated development of functional materials (materials synthesis and discovery). Although historically applied to pharmaceutical research, there is increasing interest in applying CM to materials science, as indicated by recent reports of combinatorial methodologies for a wide range of organic/polymeric materials [1–17].

Interface directed phase segregation and phase-separated microstructure are important properties of thin (1 to 1000 nm) polymer blend films. A precise understanding of phase separation phenomena in confined or reduced dimensions is crucial for the preparation of nanometer scale functional materials from multicomponent polymer blends. However, phase behavior in thin films is inherently complex due to its dependence on a large number of parameters, including molecular mass, polymer–polymer and polymer–surface interactions, temperature ( $T$ ), composition ( $\phi$ ), and film thickness ( $h$ ) [1–3,18–25]. In addition, these multiple variables interact in a complex fashion by phenomena that include surface segregation of one blend component, shift of the phase boundary with film thickness [18,21], substrate interactions, film viscosity increases or decreases relative to the bulk [4,5], and coupling between phase separation and surface deformation modes [23]. A simple estimate of possible variable combinations based on realistic ranges

of temperature ( $15^{\circ}\text{C} < T < 180^{\circ}\text{C}$ ,  $\Delta T = 2^{\circ}\text{C}$ ), mass fraction ( $0 < \phi < 1$ ,  $\Delta\phi = 0.01$ ), and thickness ( $1 \text{ nm} < h < 1000 \text{ nm}$ ,  $\Delta h = 15 \text{ nm}$ ) yields nearly 1.5 million unique  $T$ - $\phi$ - $h$  data points for a single polymer blend pair. The additional dependence on time, variations in molecular mass and chemistry, copolymerization, and extension to multicomponent mixtures causes the magnitude of unexplored variable space to become overwhelming. Faced with the large number of variable combinations and interactive phenomena, unraveling the  $T$ - $\phi$ - $h$  dependence of the kinetics and thermodynamics of thin-film phase behavior is indeed a challenging task using the conventional one-sample-for-one-measurement approach.

Early efforts in combinatorial materials science used sputtering methods to prepare composition-gradient libraries for measuring the phase behavior of ternary metal alloys [25] and other inorganic materials [26]. However, limitations in computational capability and robotics for instrument automation have severely limited the benefits of combinatorial materials characterization until recently [10–17,25]. The primary limitation to characterizing polymer thin films with combinatorial methods has been a shortage of techniques for preparing libraries with systematically varied composition  $\phi$ , thickness  $h$ , and processing conditions, e.g.,  $T$ . In a previous study, we reported a  $T$ -gradient heating stage and a velocity-gradient coating procedure that was used to prepare  $T$ - $h$  gradient film libraries to investigate dewetting and block copolymer segregation in nanoscale polymer films [7–9]. Here, we apply the gradient technique to investigate the thickness dependence of binary polymer-blends phase separation in nanoscale thin films.

We briefly review recent advances in applying CM to library design and characterization of polymer-blends phase behavior and characterization. We present applications of several novel CM developed by the authors for the preparation of  $T$ ,  $\phi$ ,  $h$ , and surface energy ( $\gamma_{so}$ ) continuous polymer film libraries. We focus in particular on the novel library preparation and high throughput screening steps, since these have been the principal limiting factors in CM development for polymers. The use of continuous-gradient libraries in the measurement of fundamental properties is described for polymer-blends phase behavior.

## 5.2 PREPARATION OF POLYMER THIN-FILM LIBRARIES

### 5.2.1 Overview

In investigations of polymer films and coatings libraries with variations in  $\phi$ ,  $h$ ,  $T$ , and,  $\gamma_{so}$ , we have found that the deposition of films with continuous gradients of these properties is a convenient and practical alternative to the deposition of libraries containing discrete regimes. However, this experimental design has the associated caveat that the scale of the continuous gradients in these libraries should accommodate point measurements and prevent cross talk between the measurement elements. Of course, the introduction of chemical, thickness, and thermal gradients drives nonequilibrium transport processes that will eliminate the gradients over very long periods of time. The timescale and lengthscale over which gradient library measurements are valid are determined in part by the magnitude of these

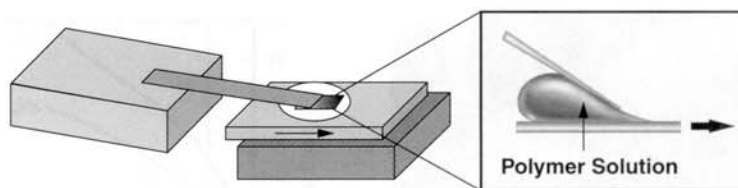


**Figure 5.1** Schematic of the combinatorial experimental method for preparation of thickness gradients. The substrate is accelerated across the knife-edge, creating a gradient in film thickness.

transport fluxes. In most cases high molecular mass<sup>1</sup> ( $M_w > 10000$  g/mol) polymers have relatively low transport coefficients, e.g., diffusivity, and high viscosity. Thus the mass transport, flow length, and time scales are often several orders of magnitude less than those of the measurements, allowing properties to be measured near equilibrium.

### 5.2.2 Thickness-Gradient Libraries

A velocity-gradient knife-edge flow coater [14–17], depicted in Figure 5.1, was developed to prepare coatings and thin films with a continuous thickness gradient. A 50  $\mu\text{L}$  drop of polymer solution (mass fraction 2% to 5%) was placed under a knife-edge with a 2.5-cm-wide stainless-steel blade, positioned at a height of 300  $\mu\text{m}$  and at a 5° angle with respect to the substrate. A computer-controlled motion stage (Parker Daedal) moves the substrate under the knife-edge at a constant acceleration, usually 0.5 to 1  $\text{mm/s}^2$ . This causes the stage velocity to gradually increase from zero to a maximum value of 5 to 10  $\text{mm/s}$ . The increasing substrate velocity results in a progressive increase in the residual fluid volume passing under the knife edge (inertial effect) giving films with controllable thickness gradients. Figure 5.2 shows an  $h$ -gradient obtained immediately after flow coating for polystyrene (PS) as a function of solute concentration on a 4-inch Si substrate. The immediately evident variation in shade shows the systematic variation of film thickness from approximately 20 nm to 100 nm across the substrate. Thin film thickness-dependent phenomena can be investigated from nanometers to micrometers employing several  $h$ -gradient films with overlapping gradient ranges. The relatively weak thickness and temperature gradients do not induce appreciable flow in the polymer film over the experimental timescale. [14,15] A unidirectional Navier–Stokes model for flow over a flat plate estimates lateral flow at a characteristic velocity of 1  $\mu\text{m/h}$  at  $T = 135^\circ\text{C}$ , in response to gravitational action on the thickness gradient [27]. This small flow is several orders of magnitude slower than the flow induced by the physical phenomena that these libraries are designed to investigate, such as dewetting [15]

<sup>1</sup>According to ISO 31–8, the term “molecular weight” has been replaced by “relative molecular mass,” symbol  $M_r$ . The conventional notation, rather than the ISO notation, has been employed for this publication.

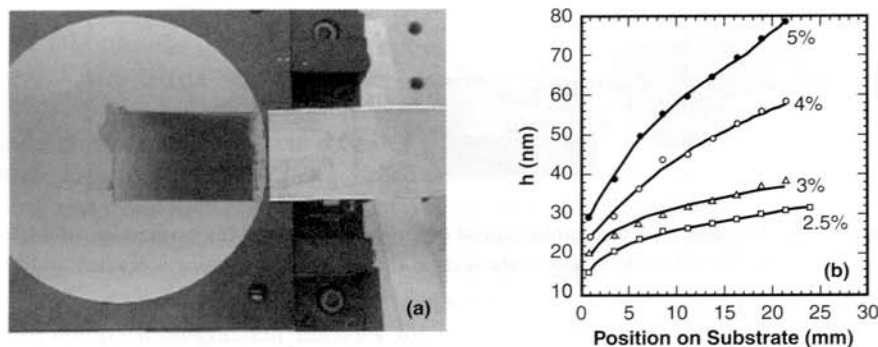


**Figure 5.2** (a) A gradient thickness film on a 4-inch Si substrate immediately after flow coating. The knife-edge and the translation stage are shown. The variation in color of the film corresponds to thickness changes from 20 nm to 100 nm, approximately. (b) Thickness,  $h$  (nm) vs.  $x$  position on substrate (mm), for various  $h$ -gradient film libraries composed of polystyrene ( $M_w = 1800$  g/mol) on Si as a function of mass fraction PS in the toluene coating solution. Standard uncertainty in thickness is  $\pm 3$  nm. (Courtesy of the National Institute of Standards and Technology, Gaithersburg, MD.)

and phase separation [14]. To check for flow, we examined thickness-gradient libraries before and after annealing at  $T > T_g$ , as shown in Figure 5.3 for a PS film ( $M_w = 1800$ ) on Si/SiO<sub>x</sub>. The difference of thickness gradients across the 2-cm  $\times$  3-cm library area before and after annealing was within a standard uncertainty of  $\pm 1.5$  nm [15].

### 5.2.3 Composition-Gradient Libraries

Three steps are involved in preparing composition gradient films: gradient mixing (Figure 5.4a), gradient deposition (Figure 5.4b), and film spreading (Figure 5.4c). Gradient mixing utilizes two syringe pumps (Harvard PHD2000)<sup>2</sup> that introduce and withdraw polymer solutions (of mass fraction  $x_A = x_B = 0.05$  to 0.10) to and from a small mixing vial at rates  $I$  and  $W$ , respectively. Pump  $W$  was used to load the vial with an initial mass  $M_o$  of solution  $B$  ( $M_o \approx 1$  g). The infusion and withdrawal syringe pumps were started simultaneously under vigorous stirring of the vial solution, and a third syringe,  $S$ , was used to manually extract  $\approx 50$   $\mu$ L of solution from the vial into the syringe needle at the rate of  $S = (30$  to  $50)$   $\mu$ L/min. At the end of the sampling process, the sample syringe contained a solution of polymers  $A$  and  $B$  with a gradient in composition,  $\nabla x_A$ , along the length of the syringe needle.

<sup>2</sup>Certain equipment and instruments or materials are identified in the chapter in order to adequately specify the experimental details. Such identification does not imply recommendation by the National Institute of Standards and Technology, nor does it imply the materials are necessarily the best available for the purpose.

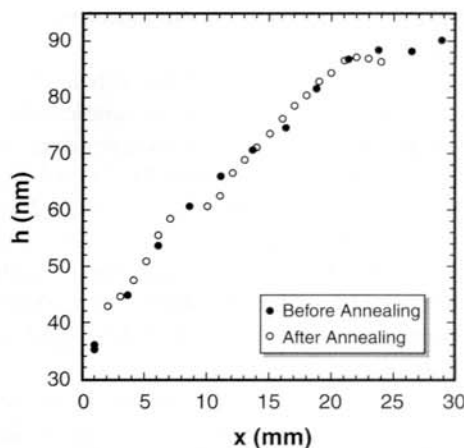


**Figure 5.3** Thickness gradients for PS ( $M_w = 1800$ ) on Si/SiO<sub>x</sub> before and after heating at 135°C for 2 h. There is no observable change in the gradient due to flow during annealing.

The relative rates of  $I$  and  $W$  were used to control the steepness of the composition gradient, e.g.,  $dx_A/dt$ . The sample time,  $t_s$ , determines the endpoint composition of the gradient. The gradient produced by a particular combination of  $I$ ,  $W$ ,  $S$ ,  $M_o$ , and  $t_s$  values was modeled by a mass balance of the transient mixing process, given elsewhere [21]. This balance predicts that the composition gradient will be linear only if  $I = (W + S)/2$ , a prediction supported by Fourier transform infrared (FTIR) measurements of composition. An 18-gauge needle long enough to contain the sample volume ensured that the gradient solution did not enter the syringe itself. This

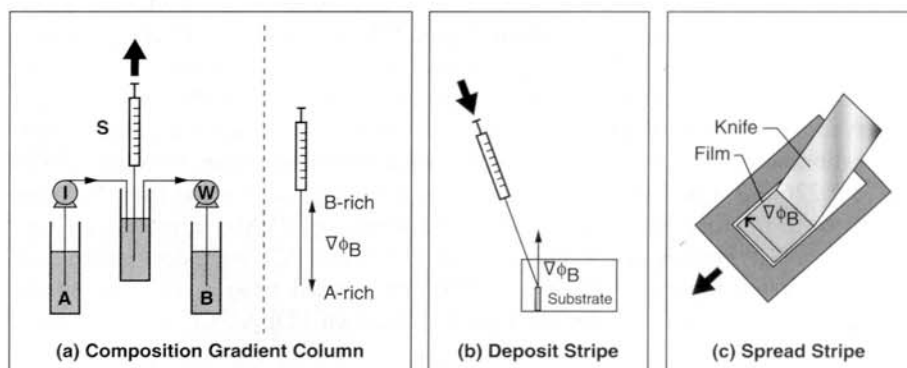


**Figure 5.4** Schematic of the composition-gradient deposition process involving (a) gradient mixing, (b) deposition of stripe, and (c) film spreading. (Figure courtesy of the National Institute of Standards and Technology, Gaithersburg, MD.)

prevented turbulent mixing that might occur upon expansion of the solution from the needle into the larger-diameter syringe.

Under the influence of the gradient in the syringe needle,  $\nabla x_A$ , molecular diffusion will homogenize the composition. However, the timescale for molecular diffusion is many orders of magnitude larger than the sampling time. For example, consider gradient solutions of PS ( $M_w = 96.4$  kg/mol,  $M_w/M_n = 1.01$ , Tosoh Inc.) and poly(vinylmethyl ether) (PVME) ( $M_w = 119$  kg/mol,  $M_w/M_n = 2.5$ ) in toluene, a system used to characterize the  $\phi$ -gradient-deposition procedure [14,28]. For a typical  $\phi$ -gradient with  $\Delta\phi \approx 0.025$  mm<sup>-1</sup>,  $\phi_{PS}$  and  $\phi_{PVME}$  change negligibly by 0.004% and 0.001% in the 5 min required for film deposition.<sup>3</sup> Fluid flow in the sample syringe remains in the laminar regime, preventing turbulence and convective mixing, as discussed elsewhere [14].

The next library preparation step (Figure 5.4b) is to deposit the gradient solution from the sample syringe as a thin stripe, usually 1 to 2 mm wide, on the substrate. This gradient stripe was then spread as a film (Figure 5.4c) orthogonal to the composition gradient using the knife-edge coater described earlier. After a few seconds most of the solvent evaporated, leaving behind a thin film with a gradient of polymer composition. The remaining solvent was removed under vacuum during annealing, described in the next section (*T*-gradient annealing). Because polymer melt diffusion coefficients,  $D$ , are typically of order 10<sup>-12</sup> cm<sup>2</sup>/s, diffusion in the cast film can be neglected if the lengthscale resolved in measurements is significantly larger than the diffusion length,  $\sqrt{Dt}$ . Composition-gradient films of blends of PS/PVME [21] and poly(D,L-lactide) (PDLA; Alkermes, Medisorb 100DL;  $M_w = 127,000$  g/mol,  $M_w/M_n = 1.56$ )/poly( $\epsilon$ -caprolactone) (PCL, Aldrich,  $M_w = 114,000$  g/mol,  $M_w/M_n = 1.43$ ) [29] were used to test the  $\phi$ -gradient procedure. The composition variation was typically verified by FTIR spectra measured with a Nicolet Magna 550 and were averaged 128 times at 4 cm<sup>-1</sup> resolution. The beam diameter, 500  $\mu$ m (approximate), was significantly larger than the diffusion length of 3  $\mu$ m (approximate) for the experimental timescale. Films 0.3 to 1  $\mu$ m thick were coated on a sapphire substrate and a translation stage was used to obtain spectra at various positions on the continuous  $\phi$ -gradient. Figure 5.5a shows typical FTIR spectra for a  $\phi$ -gradient film of PS/PVME. As position is scanned along the film, a monotonic increase in PVME absorbances, and a corresponding decrease in PS absorbances, is observed. For the PS/PVME blend, compositions were measured based upon a direct calibration of the  $\nu = 2820$  cm<sup>-1</sup> peak using known mixtures, yielding  $\epsilon(2820$  cm<sup>-1</sup>) =  $226 \pm 3 A/hc$ , where  $A$  = absorbance for this peak,  $h$  is the film thickness measured in micrometers, and  $c$  is the molar density of PVME in moles per liter. For PDLA/PCL system,  $\epsilon(\nu)$  values for pure PDLA and PCL were determined over the C-H stretch regime of (2700 to 3100) cm<sup>-1</sup>, based upon  $\epsilon_i(\nu) = A_i(\nu)/(ch)$ , where  $A_i$  is the absorbance for each peak. Unknown PDLA/PCL mass fractions

<sup>3</sup>The diffusive flow rate of PS and PVME were calculated as  $J = L\pi r^2 D_p \rho (d\phi/dx)_{\max}$ , where  $\rho$  is the solution density,  $r = 2.3$  mm is the syringe diameter, and  $L = 4.2$  mm is the length of the fluid column in the syringe. We estimate  $\Delta\phi_i$  as  $(Jt)/(x_p L \pi r^2 \rho)$ , where  $x_p = 0.08$  is the total polymer mass fraction in solution.

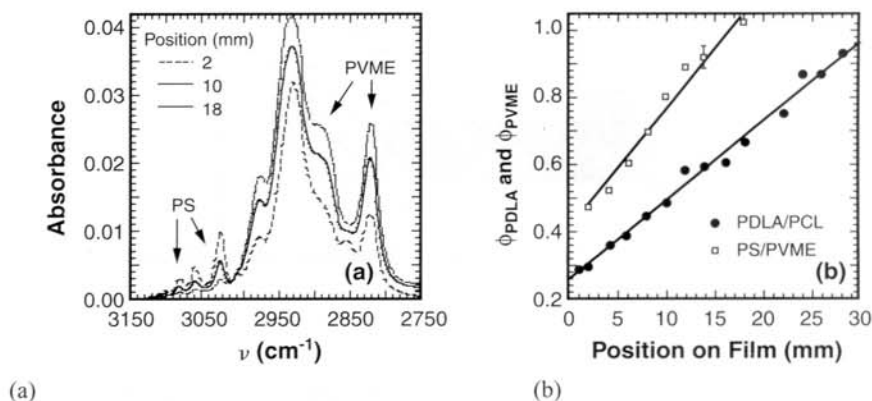


**Figure 5.5** (a) FTIR spectra at various positions  $x$  (mm) along a  $\phi$ -gradient PS/PVME library, as described in the text. PS absorptions decrease and PVME absorptions increase, monotonically, as one samples spectra across the film. (b) Mass fractions  $\phi_{\text{PVME}}$  and  $\phi_{\text{PCL}}$  vs. position,  $x$  (mm), for typical PCL/PDLA and PS/PVME  $\phi$ -gradient libraries. Composition of PS/PVME blends is calculated by calibration of the  $\nu = 2820 \text{ cm}^{-1}$  PVME absorption. Coating parameters were: PS/PVME ( $I = 0.51 \text{ mL/min}$ ,  $W = 1.0 \text{ mL/min}$ ,  $S = 20 \text{ }\mu\text{L/min}$ ,  $M_o = 1.57 \text{ mL}$ , sample time = 94 s) and PDLA/PCL ( $I = 0.76 \text{ mL/min}$ ,  $W = 1.5 \text{ mL/min}$ ,  $S = 26 \text{ }\mu\text{L/min}$ ,  $M_o = 1.5 \text{ mL}$ , sample time = 95 s) Unless otherwise indicated by error bars, standard uncertainty is represented by the symbol size. (Figure 5.5b courtesy of the National Institute of Standards and Technology, Gaithersburg, MD.)

were determined to within a standard uncertainty of 4% by assuming the observed spectra were linear combinations of pure PDLA and PCL spectra, e.g.,  $A_{\text{mix}} = h(\alpha \epsilon_{\text{PDLA}} c_{\text{PDLA}} + (1 - \alpha) \epsilon_{\text{PCL}} c_{\text{PCL}})$  and  $\alpha$  is related to the mass fraction PDLA. Figure 5.5b shows typical composition gradients for PDLA/PCL blends coated from  $\text{CHCl}_3$  and PS/PVME blends coated from toluene. Essentially linear gradients were obtained and the endpoints and slope agree with those predicted from mass balance [14]. It is possible to create gradient films with wider composition ranges than those shown in Figure 5.5, by sampling the mixing vial, Figure 5.4a, for longer times.

#### 5.2.4 Temperature-Gradient Libraries

To explore a large temperature ( $T$ ) range, the  $h$ - or  $\phi$ -gradient films are annealed on a  $T$ -gradient heating stage, with the  $T$ -gradient *orthogonal* to the  $h$ - or  $\phi$ -gradient. This custom aluminum  $T$ -gradient stage, shown in Figure 5.6, uses a heat source and a heat sink to produce a linear gradient ranging between adjustable endpoint temperatures. Endpoint temperatures typically range from  $160 \pm 0.5^\circ\text{C}$  to  $70.0 \pm 0.2^\circ\text{C}$  over 40 mm, but are adjustable within the limits of the heater, cooler, and maximum heat flow through the aluminum plate. To minimize oxidation and convective heat transfer from the substrate, the stage is sealed with an O-ring, glass plate, and vacuum pump. Each two-dimensional  $T$ - $h$  or  $T$ - $\phi$  parallel library contained about 1800 or 3900 state points, respectively, where a “state point” is defined

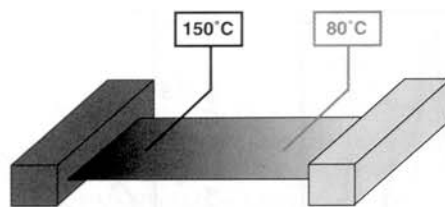


**Figure 5.6** Schematic of the temperature-gradient stage, highlighting a typical temperature range investigated.

by the  $T$ ,  $h$ , and  $\phi$  variation over the area of a  $200\times$  optical microscope image:  $\Delta T = 0.5^\circ\text{C}$ ,  $\Delta h = 3\text{ nm}$ , and  $\Delta\phi = 0.02$ . These libraries allow  $T$ ,  $h$ , and  $\phi$ -dependent phenomena, e.g., dewetting, order–disorder, and phase transitions, to be observed in situ or post-annealing with relevant microscopic and spectroscopic tools.

### 5.2.5 Surface-Energy Gradients

In many polymer-coating and thin film systems, there is considerable interest in studying the film stability, dewetting, and phase behavior on substrates with surface energies varying between hydrophilic and hydrophobic extremes. Therefore, a gradient-etching procedure has been developed in order to produce substrate libraries with surface energy,  $\gamma_{so}$ , continuously varied from hydrophilic to hydrophobic values [30]. The gradient-etching procedure involves immersion of a passivated Si-H/Si substrate (Polishing Corporation of America) into an  $80^\circ\text{C}$  Piranha solution [31] at a constant immersion rate. The Piranha bath etches the Si-H surface and grows an oxide layer,  $\text{SiO}_x/\text{SiOH}$ , at a rate dependent on  $T$  and the volume fraction  $\text{H}_2\text{SO}_4$  [31]. A gradient in the conversion to hydrophilic  $\text{SiO}_x/\text{SiOH}$  results from one end of the wafer with increasing time of exposure to the Piranha solution along the length. After immersion, the wafer is withdrawn rapidly ( $\approx 10\text{ mm/s}$ ), rinsed with deionized water, and blow-dried with nitrogen.

We have also developed a simple method for chemical modification of chlorosilane self-assembled monolayers (SAMs) on Si surfaces by exposure to a gradient in UV-ozone radiation to create stable surface energy gradient substrates. Typical deionized water contact angles are shown in Figure 5.7. By preparing several gradient substrates covering overlapping ranges of hydrophilicity, it is possible to screen a large range in surface energy, from hydrophilic ( $\theta_w \approx 0^\circ$ ) to hydrophobic ( $\theta_w \approx 90^\circ$ ) values of the water contact angle. In another procedure for varying substrate energy, mixed SAMs of alkanethiolates are deposited with a composition gradient [32]. In this procedure,  $\omega$ -substituted alkanethiolates with different terminal groups, e.g.,  $-\text{CH}_3$  vs.  $-\text{COOH}$ , cross-diffuse from the opposite ends of a polysaccharide matrix deposited on top of a gold substrate. Diffusion provides for the formation of a SAM with a concentration gradient between the two thiolate species from one end of the substrate to another, resulting in controllable substrate energy gradients. The

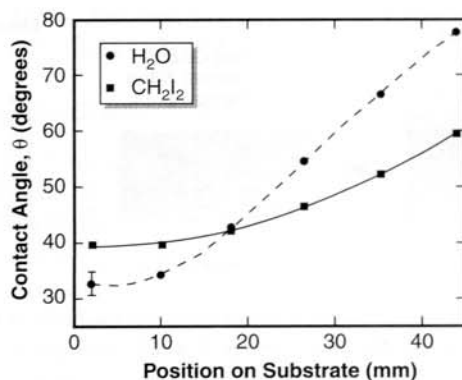


**Figure 5.7** Deionized water and diiodo methane contact angle versus spatial position (mm) for a gradient UV oxidized SAM substrate. The method allows a systematic variation of contact angles and corresponding surface energy across the substrate.

polysaccharide matrix is removed after a period of time, halting the diffusion process. These gradient SAM substrates were subsequently used to investigate the effect of surface energy on phase separation of immiscible polymer blends [33].

### 5.3 UNCERTAINTY AND STATISTICAL CONSIDERATIONS OF LIBRARY MEASUREMENTS

A potential drawback of the method is that the polymer-surface libraries are not composed of distinct sample areas, but rather have continuous gradients in  $\phi$  and annealing  $T$ . These gradients induce variance in observed properties, which is not an issue with uniform samples. Many properties measured with combinatorial libraries are obtained from microscope images [optical, fluorescent, atomic force (AFM),] or spectroscopy (UV, FTIR). Thus it is important to understand how uncertainties associated with the gradients and the lateral resolution affects properties measured on the libraries. Figure 5.8 demonstrates how a combinatorial library is divided into a grid of “virtual” measurement sites (e.g., microscope images) of lengthscale  $L$ . The  $T$  and  $\phi$  for each measurement site is taken as the average  $\langle T \rangle$  and  $\langle \phi \rangle$  over the length  $L$ . Because gradients are present on the library, each measurement site has systematic variances  $\Delta\phi$  and  $\Delta T$  that increase as the measurement lengthscale  $L$  increases. Hence lower measurement resolution (lower  $L$ ) results in lower  $\Delta\phi$  and  $\Delta T$ . A typical  $500\text{-}\mu\text{m} \times 500\text{-}\mu\text{m}$  image would have reasonable variances of  $\Delta\phi = 0.01$  and  $\Delta T = 0.3^\circ\text{C}$ . The number of measured features decreases as  $L$  decreases, causing an increase in measurement uncertainty.

A key question to be answered is how to select the optimum measurement scale  $L$ , reflecting a balance between counting statistics,  $\Delta\phi$  and  $\Delta T$ . The effects of these

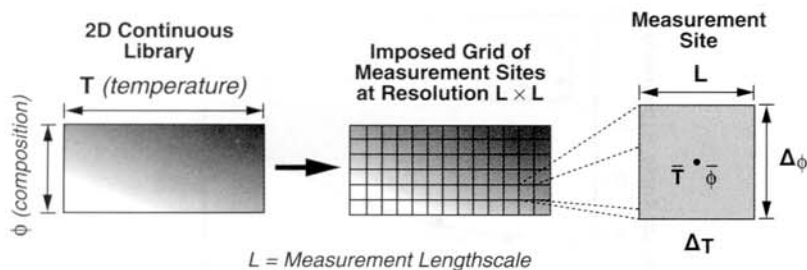


**Figure 5.8** Distribution of discrete measurement sites of resolution  $L \times L$  over a continuous gradient library. Measurement sites have average  $T$  and  $\phi$ , with gradient variance  $\Delta T$  and  $\Delta\phi$ .

contributions on the variance about the mean of any property  $\langle p \rangle$  within a measurement site is accounted for using a standard uncertainty propagation,

$$\Delta\langle p \rangle = (\partial\langle p \rangle/\partial N)\Delta N + (\partial\langle p \rangle/\partial T)\Delta T + (\partial\langle p \rangle/\partial\phi)\Delta\phi. \quad (5.1)$$

Here  $\langle p \rangle$  is a function of  $T$ ,  $\phi$ , and the number of observations made in the measurement site,  $N \sim L^2$ . It is assumed that the number of features (microstructures, cells, etc.) can be counted exactly, so that  $\Delta N = 0$ . The partial derivatives can be estimated from finite difference approximations of the measured data, e.g.,  $\partial\langle p \rangle/\partial T = (\Sigma p(T_{i+1}, \phi_i) - \Sigma p(T_i, \phi_i))/[N(T_{i+1} - T_i)]$ . The values of  $\Delta\phi$  and  $\Delta T$  are  $\Delta\phi = m_\phi L$  and  $\Delta T = m_T L$ , where  $m_T$  and  $m_\phi$  are the slopes of the linear gradients, known from the library preparation procedure. Making these substitutions shows that the error propagation for property  $p$  scales as

$$\Delta\langle p \rangle \sim (m_T + m_\phi)/L. \quad (5.2)$$

Constants have been removed in order to reveal only the dependence on gradients and the measurement scale,  $L$ . Equation (5.1) demonstrates that the uncertainty of any property measured on the libraries at a given  $\phi$  and  $T$  will decrease if the measurement scale  $L$  is increased (because more features are counted) and if the magnitude of the gradients is decreased (reducing  $\phi$  and  $T$  uncertainty). Thus the following guidelines will be followed during experimental design and data analysis: (1)  $L$  will be made as large as possible while still being able to resolve features of interest, and (2) the gradient slopes will then be adjusted to attain an acceptable uncertainty ( $<1\%$ ) in the measured property. The preceding analysis considers only uncertainty contributions from the library gradients. Additional sources of uncertainty, treated later, arising from the culturing and assay steps themselves, are also present for uniform conventional samples.

## 5.4 FUNDAMENTAL PHASE BEHAVIOR AND PROPERTIES OF POLYMER-BLEND FILM LIBRARIES

### 5.4.1 Composition Gradients for Phase Boundary

Figure 5.9 presents a photographic image of a typical temperature-composition library of the PS/PVME blend (just discussed in the composition-gradient preparation section) for 16-h annealing time. As Figure 5.9 indicates, the lower critical solution temperature (LCST) cloud-point curve can be seen with the unaided eye as a diffuse boundary separating one-phase and two-phase regions. Cloud points measured on bulk samples with conventional light scattering are shown as discrete data points and agree well with the cloud-point curve observed on the library [14,34]. The diffuse nature of the cloud-point curve reflects the natural dependence of the microstructure evolution rate on temperature and composition. Near the LCST boundary the microstructure size gradually approaches optical resolution limits ( $1\ \mu\text{m}$ ), giving the curve its diffuse appearance. Based upon a bulk diffusion coefficient of  $D \approx 10^{-17}\ \text{m}^2/\text{s}$ , the diffusion length ( $\sqrt{Dt}$ ) for a 2-h anneal is  $270\ \text{nm}$ . In Figure 5.9 each pixel covers about  $30\ \mu\text{m}$ , which is over 100 times the diffusion length, and  $\phi$ -gradient-induced diffusion has a negligible effect on the observed LCST cloud-point curve. The combinatorial technique employing  $T$ - $\phi$  polymer-

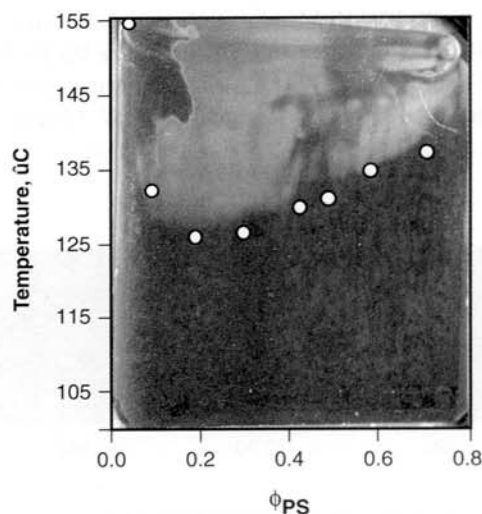


**Figure 5.9** Digital optical photographs of a PS/PVME  $T$ - $\phi$  library after 91 min of annealing, showing the LCST cloud point curve visible to the unaided eye. The library wafer dimension is  $31\ \text{mm} \times 35\ \text{mm}$  and the film thickness varies from approximately 400 to 600 nm from low to high  $\phi_{\text{PS}}$  values. White circles light-scattering cloud points measured on separate uniform samples. (Figure courtesy of the National Institute of Standards and Technology, Gaithersburg, MD.)

blend libraries represents a powerful means for rapid and efficient characterization of polymer-blend phase behavior in orders of magnitude less time than with conventional light- or neutron-scattering techniques. A large database of phase behavior of a host of binary polymeric mixtures, and the influence of additives, fillers, or other processing variables can be thus generated with tremendous implications for application of multicomponent-blend films.

#### 5.4.2 Influence of Substrate Surface-Energy

The presence of an interface in an ultrathin polymer-blend film guides or even significantly alters the phase-separation process. Confinement between the air and substrate interfaces and the preferential wetting of the components at the walls determines the in-plane and the surface-directed compositional distribution and the spatial scales. Genzer et al. have shown a wetting reversal transition from a symmetric three layer to an asymmetric two-layer structure with a change in substrate surface energy using compositional depth profiling with forward-recoil spectrometry (FRES) [33]. The segregation of a particular component to the polymer-substrate interface is governed by the interfacial energy resulting in a change in the compositional distribution and blend-phase microstructure. Other work points at the substrate dependence in the time evolution of the phase-separated morphology for Si, Au, and Co interfaces [35]. Gradient substrates with systematic variation of surface energy were used to probe the influence of surface energetics of the phase behavior of a model LCST PS/PVME blend at the critical composition of  $\phi_{PS} = 0.2$ . Figure 5.10 shows AFM images ( $30 \mu\text{m} \times 30 \mu\text{m}$ ) of a PS/PVME film having a fixed thickness  $h = 57 \text{ nm}$  cast on a substrate with a gradient in surface energy. The surface-energy gradient was obtained by gradient UV ozonolysis of an octyl-

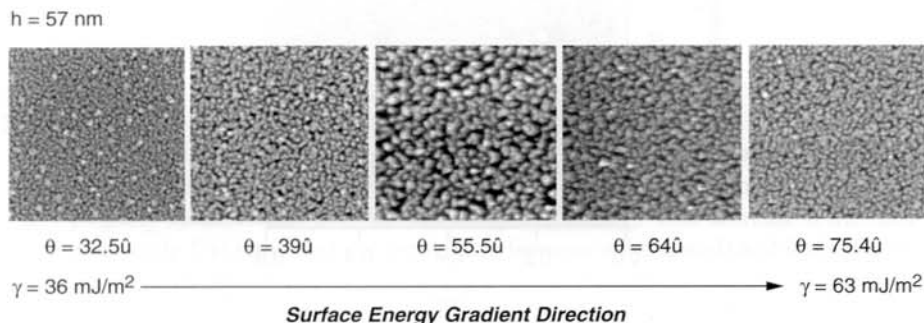


**Figure 5.10** Blend-phase morphology dependence on surface energy. AFM images of PS/PVME blend film ( $\phi_{PS} = 0.2$ ) at a constant thickness  $h = 57 \text{ nm}$  on a SAM gradient energy substrate. A nonmonotonic change in the lateral scale of phase separation is evident as we span surface-energy space. Maximal scale seen for  $\theta = 55^\circ$  corresponding to a surface energy of  $48 \text{ mJ/m}^2$ . (Figure courtesy of the National Institute of Standards and Technology, Gaithersburg, MD.)

dimethylchlorosilane SAM ( $32.5^\circ < \theta_{\text{H}_2\text{O}} < 75.4^\circ$ ;  $36 \text{ mJ m}^{-2} < \gamma_{\text{so}} < 63 \text{ mJ m}^{-2}$ ). The phase-separation process has developed to long times ( $T = 145^\circ\text{C}$ ) where “pinning” occurs. It is evident from Figure 5.10 that the pattern scale varies nonmonotonically with the surface energy of the substrate. The surface structures of the annealed films were mapped using AFM, preprogrammed to uninterruptedly map out a total of approximately 100 scans over the phase-separated film regions of interest.

Automated image analysis includes radially averaging the isotropic fast Fourier transform (FFTs) of the AFM height-topography images to give the in-plane scale of phase separation,  $\lambda$ . We observe that the pattern scale ( $\lambda$ ) is maximum for an intermediate characteristic value of  $\gamma^* = 48 \text{ mJ m}^{-2}$  ( $\theta = 55^\circ$ ) that is nearly independent of  $h$ . We tentatively assign this value of  $\gamma^* = 48 \text{ mJ m}^{-2}$  to the surface energy where both polymer components of the blend have a similar polymer–substrate interaction and the effective film thickness is maximal with the depletion of the substrate–polymer boundary layer. Measurement of polymer–substrate interactions is key to understanding the stability and phase behavior of polymer with blend films on surfaces. The continuous-gradient approach provides this information in an efficient manner without involving numerous substrates with creating incremental variations of surface energy and characterizing the surface energy of each substrate.

### 5.4.3 Film-Thickness Gradients

Figure 5.11 shows the progressive change of scale of the late stage of phase separation morphology with increasing film thickness for the PS/PVME film at fixed surface energy,  $\gamma_{\text{so}} = 63 \text{ mJ m}^{-2}$ . This  $h$ -gradient range is low enough ( $< 200 \text{ nm}$ ) that surface-directed spinodal decomposition is suppressed, and phase separation occurs laterally [24]. In addition,  $h > 2R_g$ , where  $R_g = 8 \text{ nm}$ , is the estimated radius of gyration of the polymers. Hence the film is not confined completely to two dimensions,

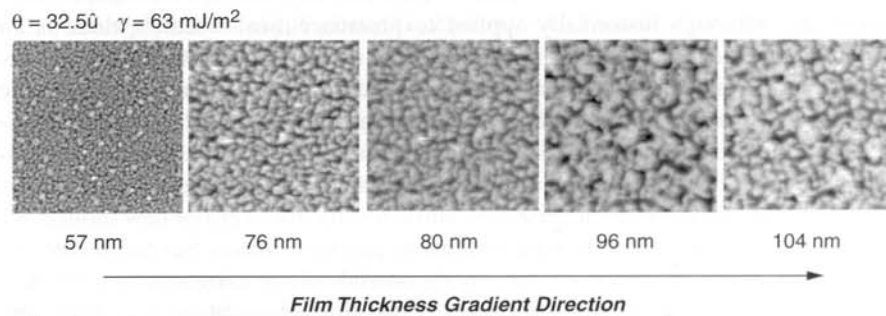


**Figure 5.11** Blend-phase morphology dependence on film thickness. AFM images of PS/PVME ( $\phi_{\text{PS}} = 0.2$ ) blend-phase morphology at a constant surface energy  $\gamma_{\text{so}} = 63 \text{ mJ/m}^2$  for a gradient thickness film. A systematic increase in the lateral scale of phase separation is evident with film thickness. (Figure courtesy of the National Institute of Standards and Technology, Gaithersburg, MD.)

but is in a transition regime between a three-dimensional (bulk) and two-dimensional geometry. Figure 5.11 shows that thickness has a profound effect on microstructure size, film topography, and roughness. A bicontinuous lateral microstructure superimposed upon a topography of peaks and valleys is observed at all  $h$ -values. This bicontinuous structure is consistent with phase separation in the spinodal regime, and the peak and valley topography has been attributed to surface-tension differences between PS-rich and PVME-rich regions. The pattern scale  $\lambda$  is determined by FFTs of the AFM height images of the patterns. No statistically significant variation of  $\lambda$  was determined by changing scan dimensions. We observe a linear increase of  $\lambda$  with increasing film thickness,  $h$ . There have been some recent studies to indicate this behavior in phase separation in thin films [36–38]. However, other work has also suggested nonlinear trends depending on the blend chemistry and experimental conditions [36]. Care must be taken to generalize results, since the behavior can change significantly with substrate surface energy or in other film-thickness regimes where changes in phase-separation kinetics are anticipated. The nonmonotonic variation of lateral scale with substrate surface energy suggests a possible explanation for the variance in observed experimental trends for different chemistries. The combinatorial approach allows us to rapidly scan for both substrate surface-energy variations and film-thickness changes in this case [39].

## 5.5 CONCLUSIONS

To allow more efficient measurement of phase behavior over large ranges of  $T$ - $\phi$ - $h$  parameter space, we report novel combinatorial library preparation and high throughput screening methods for nanoscale polymer-blend thin films. The benefits include efficient characterization of large regimes of thermodynamic and kinetic behavior (knowledge discovery) and accelerated development of functional materials (materials discovery). This is accomplished by coupling sample libraries containing hundreds to thousands of variable combinations with high throughput measurements. Although historically applied to pharmaceutical research, there is an ongoing movement to apply this methodology in materials characterization and development, as indicated by recent reports for inorganic and organic or polymeric materials. In this chapter we have presented recent advances in which combinatorial methodologies have been used for efficient measurement of chemical and physical properties of polymer blends over large regimes of variable space. Methodologies for phase-behavior characterization allow for the discovery of new models for structure-processing-property relationships in polymer blends. Several recent developments were presented in the combinatorial characterization of polymer blends phase behavior and properties using high throughput libraries of films and coatings using continuous-gradient polymer libraries with controlled variations in temperature, composition, thickness, and substrate surface energy. The use of these new library techniques facilitates characterization of polymer-blend phase behavior, and more generally multicomponent polymeric materials.

More recently, the continuous-gradient high throughput approach has been used

for mapping phase behavior of olefinic [40], as well as nanocomposite polymer blends [41], as representative blend systems of commercial importance. These studies demonstrate the utility of the continuous-composition-gradient methods for investigating industrially important and relevant problems in phase-separated and multicomponent polymeric materials, an approach that is likely to be adopted widely by the plastics and materials manufacturing industries in the future.

## REFERENCES

1. Jandeleit, B.; Schaefer, D. J.; Powers, T. S.; Turner, H. W.; Weinberg, W. H. *Angew. Chem. Int. Ed.*, 1999, 38: 2494–2532.
2. Gravert, D. J.; Datta, A.; Wentworth, P.; Janda, K. D. *J. Am. Chem. Soc.*, 1998, 120: 9481–9495.
3. Brocchini, S.; James, K.; Tangpasuthadol, V.; Kohn, J. *J. Am. Chem. Soc.*, 1997, 119: 4553–4554.
4. Brocchini, S.; James, K.; Tangpasuthadol, V.; Kohn, J. *J. Biomed. Mater. Res.*, 1998, 42: 66–75.
5. Dickinson, T. A.; Walt, D. R.; White, J.; Kauer, J. S. *Anal. Chem.*, 1997, 69: 3413–3418.
6. Reynolds, C. H. *J. Comb. Chem.*, 1999, 1: 297–306.
7. Schmitz, C.; Posch, P.; Thelakkat, M.; Schmidt, H. W. *Phys. Chem. Chem. Phys.*, 1999, 1: 1777–1782.
8. Schmitz, C.; Thelakkat, M.; Schmidt, H. W. *Adv. Mater.*, 1999, 11: 821.
9. Schmitz, C.; Posch, P.; Thelakkat, M.; Schmidt, H. W. *Macromol. Symp.*, 2000, 154: 209–222.
10. Gross, M.; Muller, D. C.; Nothofer, H. G.; Sherf, U.; Neher, D.; Brauchle, C.; Meerholz, K. *Nature*, 2000, 405: 661.
11. Takeuchi, T.; Fukuma, D.; Matsui, J. *Anal. Chem.*, 1999, 71: 285–290.
12. Terrett, N. K. *Combinatorial Chemistry*, Oxford University Press, Oxford, 1998.
13. Kennedy, K.; Stefansky, T.; Davy, G.; Zackay, V. F.; Parker, E. R. *J. Appl. Phys.*, 1965, 36: 3808–3810.
14. Meredith, J. C.; Karim, A.; Amis, E. J. *Macromolecules*, 2000, 33: 5760–5762.
15. Meredith, J. C.; Smith, A. P.; Karim, A.; Amis, E. J. *Macromolecules*, 2000, 33: 9747–9756.
16. Smith, A. P.; Meredith, J. C.; Douglas, J. F.; Amis, E. J.; Karim, A. *Phys. Rev. Lett.*, 2001, 87: 015503.
17. Smith, A. P.; Douglas, J. F.; Meredith, J. C.; Amis, E. J.; Karim, A. *J. Polym. Sci. B: Polym. Phys.*, 2001, 39: 2141–2158.
18. Reddington, E.; Sapienza, A.; Gurau, B.; Viswanathan, R.; Sarangapani, S.; Smotkin, E.; Mallouk, T. *Science*, 1998, 280: 1735–1737.
19. Xiang, X.-D.; Sun, X.; Briceno, G.; Lou, Y.; Wang, K.-A.; Chang, H.; Wallace-Freedman, W. G.; Chen, S.-W.; Schultz, P. G. *Science*, 1995, 268: 1738–1740.
20. Wang, J.; Yoo, Y.; Gao, C.; Takeuchi, I.; Sun, X.; Chang, H.; Xiang, X.-D.; Schultz, P. G. *Science*, 1998, 279: 1712–1714.

21. Sun, X.-D.; Xiang, X.-D. *Appl. Phys. Lett.*, 1998, 72: 525–527.
22. Danielson, E.; Golden, J. H.; McFarland, E. W.; Reaves, C. M.; Weinberg, W. H.; Wu, X. D. *Nature*, 1997, 389: 944–948.
23. Danielson, E.; Devenney, M.; Giaquinta, D. M.; Golden, J. H.; Haushalter, R. C.; McFarland, E. W.; Poojary, D. M.; Reaves, C. M.; Wenberg, W. H.; Wu, X. D. *Science*, 1998, 279: 837–839.
24. Klein, J.; Lehmann, C. W.; Schmidt, H.-W.; Maier, W. F. *Angew. Chem. Int. Ed.*, 1998, 37: 3369–3372.
25. Hanak, J. J. *J. Mater. Sci.*, 1970, 5: 964–971.
26. Newkome, G. R.; Weis, C. D.; Moorefield, C. N.; Baker, G. R.; Childs, B. J.; Epperson, J. *Angew. Chem. Int. Ed.*, 1998, 37: 307–310.
27. Leal, L. G. *Laminar Flow and Convective Transport Processes*, Butterworth-Heinemann, Boston, 1992.
28. Davis, P. J.; Pinder, D. N.; Callaghan, P. T. *Macromolecules*, 1992, 25: 170–178.
29. Meredith, J. C., Amis, E. J. *Macromol. Chem. Phys.*, 2000, 201: 733–739.
30. Ashley, K.; Meredith, J. C.; Karim, A.; Raghavan, D. *Polym. Int.*, 2002, in print.
31. Kern, W., Ed. *Handbook of Semiconductor Wafer Cleaning Technology*, Noyes, Park Ridge, NJ, 1993.
32. Liedberg, B.; Tengvall, P. *Langmuir*, 1995, 11: 3821–3827.
33. Genzer, J.; Kramer, E. J. *Europhys. Lett.*, 1998, 44: 180–185.
34. Meredith, J. C.; Karim, A.; Amis, E. J. Manuscript in preparation.
35. Winesett, D. A.; Ade, H.; Rafailovich, M.; Zhu, S. *Polym. Int.*, 2000, 49: 458–462.
36. Müller-Buschbaum, Stamm, M. *Colloid Polym. Sci.*, 2001, 279: 376–381.
37. Walheim, S.; Böltau, M.; Mlynek, J.; Krausch, G.; Steiner, U. *Macromolecules*, 1997, 30: 4995–5003.
38. Dalonki-Veress, K.; Forrest, J. A.; Dutcher, J. R. *Phys. Rev. E*, 1998, 57(8): 5811–5817.
39. Sehgal, A.; Douglas, J.F.; Amis, E. J.; Karim, A. Manuscript in preparation.
40. Wang, H.; Shimizu, K.; Hobbie, E. K.; Wang, Z.-G.; Meredith, J. C.; Karim, A.; Amis, E. J.; Hsiao, B. S.; Hsieh, E. T.; Han, C.C. *Macromolecules*, 2002, 35: 1072–1078.
41. Karim, A.; Yurekli, K.; Meredith, C.; Amis, E. J., Krishnamoorti, R. *Polym. Eng. Sci.*, In Press.